International Journal of Machine Tools & Manufacture 85 (2014) 14–29

Contents lists available at ScienceDirect

International Journal of Machine Tools & Manufacture

journal homepage: www.elsevier.com/locate/ijmactool

Mechanism investigation of friction-related effects in single point incremental forming using a developed oblique roller-ball tool

B. Lu [a], Y. Fang [a], D.K. Xu [a], J. Chen [a,*], H. Ou [b], N.H. Moser [c], J. Cao [c]

[a] Department of Plasticity Technology, Shanghai Jiao Tong University, 1954 HuaShan Road, Shanghai 200030, China
[b] Department of Mechanical, Materials and Manufacturing Engineering, University of Nottingham, Nottingham NG7 2RD, UK
[c] Department of Mechanical Engineering, Northwestern University, Evanston, IL 60208, USA

ARTICLE INFO

Article history:
Received 15 March 2014
Received in revised form
18 April 2014
Accepted 22 April 2014
Available online 9 May 2014

Keywords:
Incremental forming
Friction
Tool
Through-the-thickness-shear

ABSTRACT

Single point incremental forming (SPIF) is a highly versatile and flexible process for rapid manufacturing of complex sheet metal parts. In the SPIF process, a ball nose tool moves along a predefined tool path to form the sheet to desired shapes. Due to its unique ability in local deformation of sheet metal, the friction condition between the tool and sheet plays a significant role in material deformation. The effects of friction on surface finish, forming load, material deformation and formability are studied using a newly developed oblique roller ball (ORB) tool. Four grades of aluminum sheet including AA1100, AA2024, AA5052 and AA6111 are employed in the experiments. The material deformation under both the ORB tool and conventional rigid tool are studied by drilling a small hole in the sheet. The experimental results suggest that by reducing the friction resistance using the ORB tool, better surface quality, reduced forming load, smaller through-the-thickness-shear and higher formability can be achieved. To obtain a better understanding of the frictional effect, an analytical model is developed based on the analysis of the stress state in the SPIF deformation zone. Using the developed model, an explicit relationship between the stress state and forming parameters is established. The experimental observations are in good agreement with the developed model. The model can also be used to explain two contrary effects of friction and corresponding through-the-thickness-shear: increase of friction would potentially enhance the forming stability and suppress the necking; however, increase of friction would also increase the stress triaxiality and decrease the formability. The final role of the friction effect depends on the significance of each effect in SPIF process.

1. Introduction

Incremental sheet forming (ISF) is an attractive concept for rapid manufacturing of complex sheet metal parts. It has excellent adaptability to computer numerical control (CNC) system through direct control of CAD data, minimizing the use of specialized tooling and presses. Since this process is highly flexible with low tooling cost as well as enhanced formability, it is particularly attractive for manufacturing high value-added, small batch and customized sheet metal parts especially in artificial medical replacements and aerospace industry. Since the inception of the ISF idea in 1960s by Roux and Leszak [1,2], a number of variations of the ISF process have been explored. Iseki et al. [3] developed the single point incremental forming (SPIF) process by deforming sheet metal using a ball-nose tool along a path of contour lines. Matsubara [4] proposed a two-point incremental forming (TPIF) process, in which the tool draws contours from the inside outwards while at the same time, the blank holder gradually moves downwards onto a male die. Araghi et al. [5] developed a hybrid process in which the stretch forming and asymmetric incremental sheet forming are combined together. Malhotra et al. [6] developed a double side incremental forming (DSIF) process with two moving tools. In these ISF processes, sheet metal parts with complex shapes can be formed with simple generic tools by using geometry-specific tool paths.

Although the ISF process has been researched for over 20 years, there have been limited ISF applications in the industry. This is due to a number of reasons including unsatisfactory formability, geometrical inaccuracy, long forming time, severe thinning and poor surface finish. Concerning the formability, Duflou et al. [7]

* Corresponding author. Tel.: +86 21 62813430.
E-mail address: jun_chen@sjtu.edu.cn (J. Chen).

http://dx.doi.org/10.1016/j.ijmachtools.2014.04.007

introduced laser heating in the SPIF process to increase the formability. They also extended the process window of the single point incremental forming process using multi-step tool paths [8]. Malhotra et al. [9] employed two moving tools to squeeze the sheet during the forming process in an effort to obtain higher formability and a better sheet thickness distribution. Concerning the geometrical accuracy, different approaches have been implemented, including optimizing the processing parameters, forming strategies and the tool path. Ambrogio et al. [10] analyzed the influence of different parameters relating to the accuracy and proposed a modified tool path approach to increase the dimensional accuracy. Bambach et al. [11] employed the multi-stage strategies as over-bending strategies in order to form a pyramidal benchmark part. A hybrid forming process integrating stretch forming was proposed by Araghi et al. [12]. This hybrid forming process is able to increase geometrical accuracy while also reducing forming time and relieving thinning. In ISF processes, one of the most important features is the localized deformation. The sheet is deformed locally around the contact area of tool and sheet. As the contact area is small around the tool and sheet, high contact pressure and consequently high friction may occur [13]. This may result in poor surface finish or other related issues. Thus detailed investigation of the friction effect is quite necessary for developing new methods for improved sheet surface quality and enhancing the appeal for industrial applications.

In the ISF process, surface finish may be affected by many factors including processing parameters, tool and sheet materials, and lubrication condition. Hagan and Jeswiet [14] adopted white interferometry scanning to characterize the surface finish under different depth increments and spindle speeds. The results showed an exponential increase in the maximum peak-to-valley height as the increment size decreased, and little correlation between spindle speed and roughness. However, the mechanism of friction in SPIF was not fully revealed. Hussain et al. [15] found that lubricant and lubrication method directly affect the product surface quality although the application of lubricant may not be environmentally friendly and cost-effective. Hamilton and Jeswiet [16] empirically classified the processing parameters into a speed factor and shape factor. Durante et al. [17] calculated the relationship between the roughness and ISF parameters including tool radius, vertical step depth and wall angle of the forming parts with a mathematical method, which did not take the deformation and material properties of the sheet metal into consideration. Concerning the improvement of surface quality, Lu et al. [18] developed a feature based tool path generation strategies to improve the surface quality of final part. Kim and Park [19] suggested that the roller-ball tool would improve the surface finish of the sheet during the SPIF process. Although the roller-ball tool has been proposed for years, limited research has been reported in the actual implementation of the technique. One critical problem is that the traditional vertical roller-ball (VRB) tool is limited to the maximum achievable forming angle in the SPIF process due to the interference between the tool and part. As shown in Fig. 1, this problem is especially true for the 3-Axis NC machine that is commonly used in SPIF experiment. Therefore, to develop a new tool configuration is much crucial in potentially improving the surface quality and reducing the lubricant consumption during the SPIF process.

High pressure may result in larger frictional resistance. Many researchers have suggested that friction is a major factor in contributing to the through-the-thickness-shear in the SPIF process. By using finite element analysis (FEA), Bambach et al. [13] observed the through-the-thickness-shear in the simulation and this shear is dependent on both the tool diameter and the vertical pitch. Allwood et al. [20] investigated the through-the-thickness-shear caused by the friction in the direction of tool motion. They suggested that this through-the-thickness-shear helps increase the forming limit. Eyckens et al. [21] employed an extended M–K analysis method and found that the through-the-thickness-shear would increase the formability. In the analysis, small holes were drilled in the blank and the shear angles were detected. Eyckens et al. [22] also investigated the contact shape between tool and sheet under different geometric conditions and simulated the distribution of contact stress around the plastic zone using a sub-model technique. Jackson et al. [23] investigated the incremental forming of a sandwich panel and found that the friction would cause the translation of both upper and lower surfaces along the tool motion direction. Based on the experimental measurements, Jackson and Allwood [24] suggested that SPIF was the combination of bending, stretching and shearing. Eyckens et al. [25] investigated the effect of friction in the SPIF process and suggested that through-the-thickness-shear would be affected by the tool rotation. Although these studies investigated the through-the-thickness-shear throughout the ISF process, there are still a number of open questions to be answered regarding the relationship between friction and the through-the-thickness-shear, as well as these effects on the SPIF formability.

In particular, this paper will focus on the frictional effect in SPIF process. To avoid the possible scratch on the sheet surface, an innovative oblique roller-ball (ORB) tool in combination with an NC path generation algorithm was developed. Based on the ORB tool, the effects of friction on surface finish, forming load, sheet deformation and formability have been systematically studied for four grades of aluminum sheet materials including AA1100, AA2024, AA5052 and AA6111. The material deformation behavior under both ORB tool and conventional rigid tool are investigated by drilling a small hole in the sheet while the formability is evaluated by processing a hyperbolic part. To obtain a better understanding of the frictional effect, an analytical model is developed based on stress analyses. Stress triaxiality, as an indicator to the formability, has also been calculated. Finally, the frictional effect in the SPIF process is discussed based on both the theoretical and experimental observations.

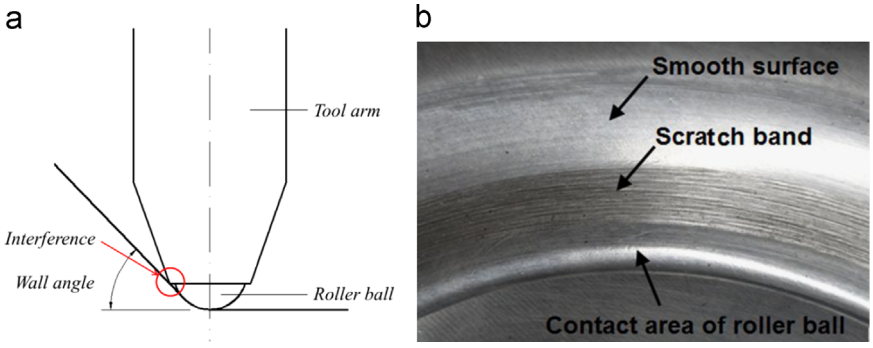

Fig. 1. VRB tool and its shortcoming. (a) Geometry of VRB tool and (b) surface scratch by VRB tool.

2. Development of an oblique roller-ball tool

2.1. ORB tool development

In conventional SPIF forming process, a ball-head rigid tool is widely used to deform the sheet to the desired shape. This tool is normally made of steel or carbide, and contacts with the sheet in hard mode. This kind of tool leaves scratches on the sheet surface, especially while processing on pure aluminum or pure titanium even under solid lubricant conditions. In order to overcome this problem, a roller-ball tool was developed to improve the surface finish of the sheet [19]. As stated in the previous section, this kind of tool is limited by the maximum achievable forming angle due to possible interferences between the tool and the inclined wall. Therefore, a new oblique roller-ball tool is proposed in this work as shown in Fig. 2. In the design, a ball cap is clamped by the tool arm in a certain angle instead of clamped vertically in the conventional design. Although the ball cap is fixed obliquely, the position of the ball cap is designed so that the center line of spindle will be across the center of roller ball. In this way, the rotation of the spindle will not change the position of the roller ball in the SPIF process.

Based on this new design, the ball head side (the front side) of tool will not interfere with the forming part even under large forming angles as shown in Fig. 3(a). By employing the rotation of spindle in a 3-Axis NC machine, the working principle is shown in Fig. 3(b). During the SPIF process, the spindle drives the forming tool to rotate according to a pre-defined NC program. The NC program is generated based on the part geometry to ensure that the ball head side of the tool always points towards the outward-normal direction of the local contact area. In this way, the interference between the part and tool can be avoided and a maximum forming angle of about 80° can be achieved.

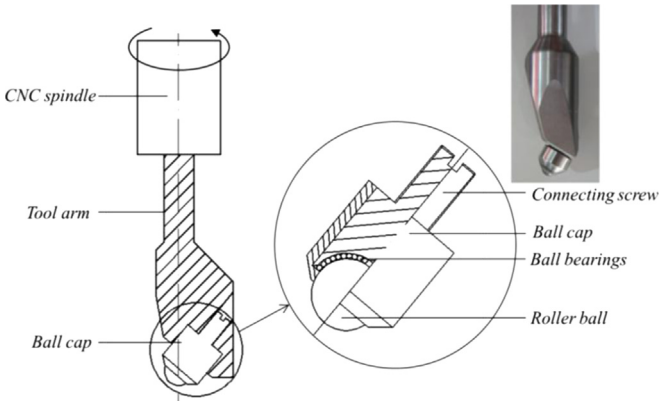

Fig. 2. The schematic and physical appearance of ORB tool.

2.2. Tool path generation algorithm

To ensure the successful implementation of the ORB tool, it is necessary to develop a specific NC program to couple the tool rotation with feed rate. As shown in Fig. 4, the ORB is initially directed towards the outward normal direction of point. For a given constant tool rotational speed ω, the duration t during which the tool moves from point A to point B can be calculated as

$$t = \frac{\alpha}{\omega} \tag{1}$$

where α is the angle between the tangential directions V_A and V_B at points A and B, respectively. In this way, α can be calculated by

$$\alpha = \arccos\left(\frac{V_A \cdot V_B}{|V_A||V_B|}\right) \tag{2}$$

The distance between points A and B is $|V_A|$, which determines to the feed rate v of the ORB tool between points A and B:

$$v = \frac{|V_A|}{t} = \frac{|V_A|}{\arccos(V_A \cdot V_B/|V_A||V_B|)}\omega \tag{3}$$

Based on the original NC tool path program generated by commercial CAM software, each sectional feed rate between two points on the tool path can be generated by using Eq. (3) under constant tool rotation speed. Then the calculated tool feed rate v can be inserted into the NC program to enable the control of the feed rate at each NC point on the path. Hence, the final program containing the tool path information can be rewritten with the front side always directed towards the normal direction of the transient contact area during forming process. The effectiveness of this method has been proven by processing a complex flower shape shown in Fig. 5(a) with the corresponding feed rate controlled by the program. Fig. 5(b) shows the final flower shape with a wall angle of approximately 45° manufactured by the ORB tool. Fig. 6 illustrates ISF forming of a truncated cone with a wall angle of 70°, which demonstrates the potential of the ORB tool regarding forming capability.

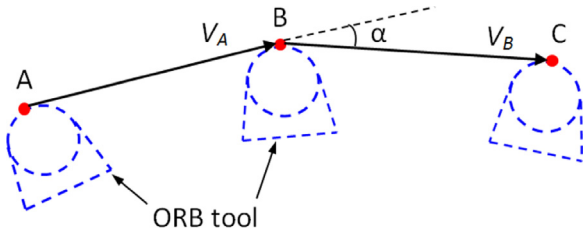

Fig. 4. The algorithm for oblique roller-ball tool.

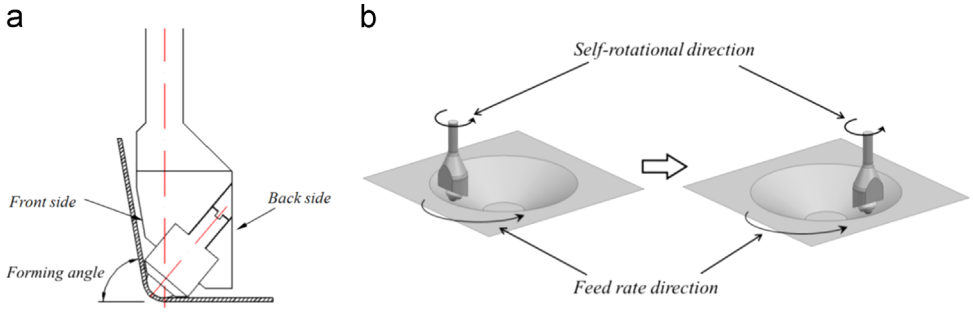

Fig. 3. The principle of larger wall-angle part forming with oblique roller-ball tool. (a) Maximum wall-angle processed by the oblique roller-ball tool and (b) the procedure of SPIF processing.

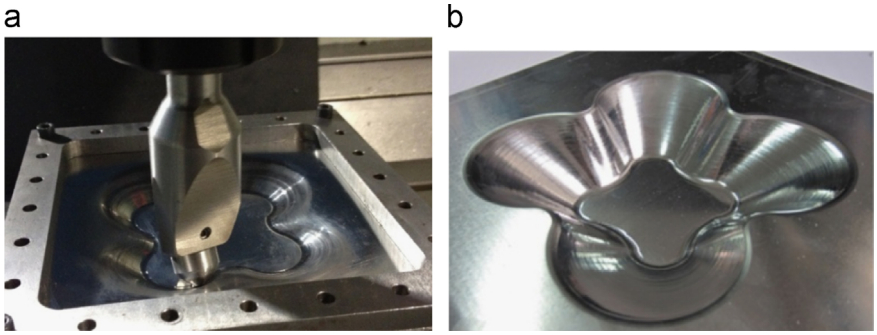

Fig. 5. A flower shape part processed by oblique tool. (a) Forming process and (b) finished part.

Fig. 6. Forming a part with wall angle of 70°.

3. Experiments

3.1. Experimental setup

In order to examine the effectiveness of the developed ORB tool and investigate the frictional effect, a series of tests have been conducted including evaluation of surface finish, forming load, deformation and fracture behavior. In the experiment, a rigid clamping frame was installed on the table of 3-Axis NC milling machine to fix the blank edges during incremental forming. Different types of forming tools including the conventional rigid tool, the VRB tool and the developed ORB tool were experimentally compared as shown in Fig. 7. The ball-end radius of the three tools is 5 mm. It is noteworthy that during the experimental process, the spindle of the machine was locked when the rigid tool was employed without self-rotation during the ISF process. Concerning the sheets employed in the experiments, different grades of aluminum alloy, including AA1100, AA2024, AA5052 and AA6111 were used in the experiments. These sheets were trimmed to the size of 180 mm × 180 mm with an initial thickness of 1 mm.

3.2. Evaluation of friction

Ahead of investigations on the frictional effect, the friction between the tool and the sheet metals during the SPIF process was evaluated by forming a U-shaped groove of 100 mm in length on an AA1100 sheet, and a zigzag tool path was implemented with incremental depth of 0.5 mm in total 16 passes as illustrated in Fig. 8. It is worth mentioning that the ORB tool was absent from this groove test. Concerning the shape of groove and the developed ORB tool, no matter in which direction the front side of the ORB tool towards during the experiment, the back side of the tool always interferes with the sheet after a certain forming depth. As the VRB tool and the ORB tool share the same ball cap unit while the only difference is from the clamping angle of the ball cap, the performance of these two tools regarding to the friction should be similar. Thus only VRB and the rigid tool are employed in this test. The similarity in friction between VRB and ORB tool can be further proven by the generated sheet surface profile in the following Section 3.3. In the forming process, a constant forming speed of 1000 mm/min was used. For the rigid tool, machine oil was used as a lubricant whereas no lubricant for VRB tool. Fig. 9 shows the friction test experiments using different tools.

The measured forming loads in Fig. 10 show the cyclical change in tool forces tends to be a U shape, which corresponds to each pass. At the two ends of a groove, the force reaches its local maximum value due to incremental feeding step downward, the force value decreases to its local minimum at the mid position of the groove. Comparing the forces generated from different tools, it is found that there is no obvious difference within the initial stages of forming. However, with the increase of forming depth, the horizontal force generated by VRB tool becomes obviously lower than that generated by rigid tool. Concerning the vertical force, the VRB tool generates a slightly larger force than those by the rigid tool at mid stage. However it becomes slightly lower after the 10th pass. The force difference suggests the varied friction conditions by using the two forming tools in SPIF process.

The friction coefficient is difficult to calculate precisely since the measured horizontal force contains not only the friction but also the forming force. Alternatively, a friction indicator μ^* is defined in the analysis to evaluate the friction condition. This approach was also employed by Xu et al. [26]. In their approach, the friction indicator was used to evaluate the friction condition in SPIF by using a rotational laser surface textured tool. The friction indicator is the ratio between the horizontal and vertical force components at the mid position of the groove in each pass, as given in the following equation:

$$\mu^* = \frac{f_H}{|f_Z|} = \frac{\text{friction} + \text{forming load}}{|f_Z|} \tag{4}$$

where f_H is the horizontal force while f_Z is the vertical force at the mid-point of each pass. In the equation, the absolute value of f_Z is taken as the negative force value outputted from the data acquisition system. It is necessary to point out that μ^* is not only determined by friction conditions but also related to other effects such as material hardening and geometry of the desired components. During the mentioned experiments, these effects are kept the consistent to minimize the disturbances to friction evaluation. The calculated friction indicators for each pass in Fig. 11 show that both friction indicators increase with the rise of forming passes, which suggests that the friction resistance is pressure dependent since the forming forces increases during the test. The change of friction can be considered as two stages:

(1) At the first stage, the friction indicator varies between 0.13 and 0.20 and there is no obvious difference of the values by using different tools.

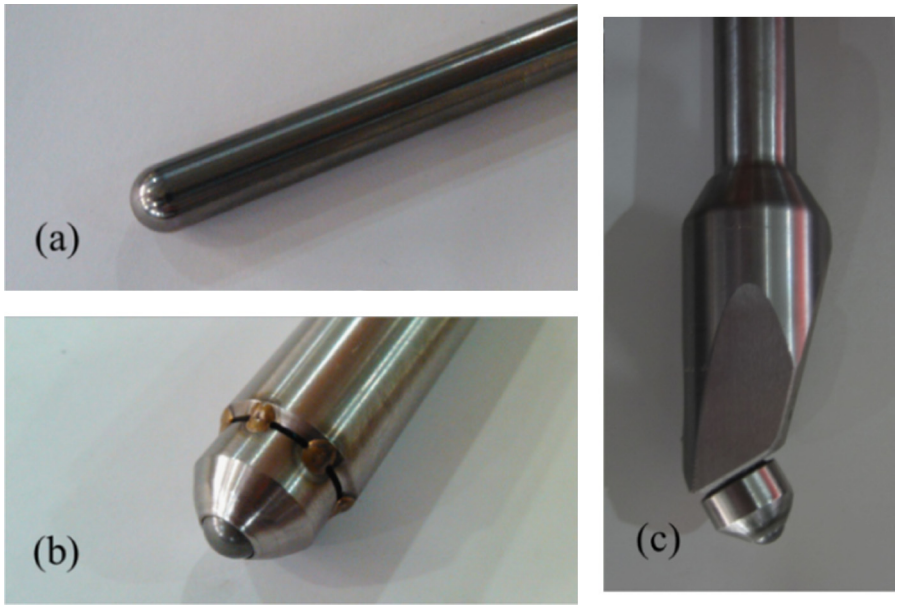

Fig. 7. Different type of tools. (a) Rigid tool, (b) VRB tool, and (c) ORB tool.

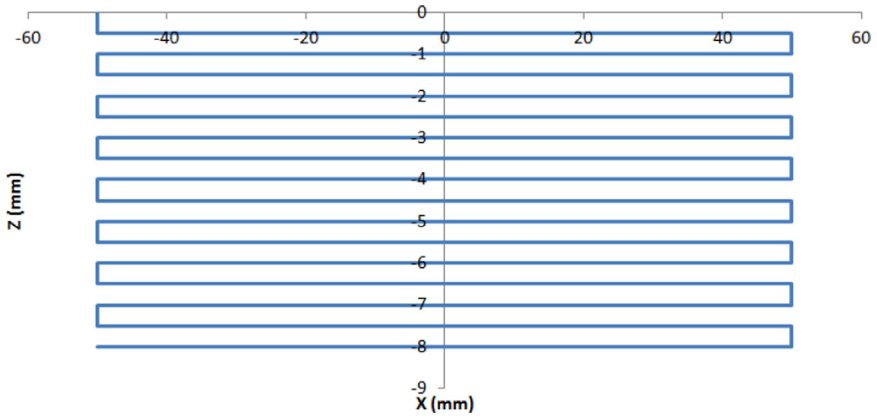

Fig. 8. Tool path for forming of the U-shape groove.

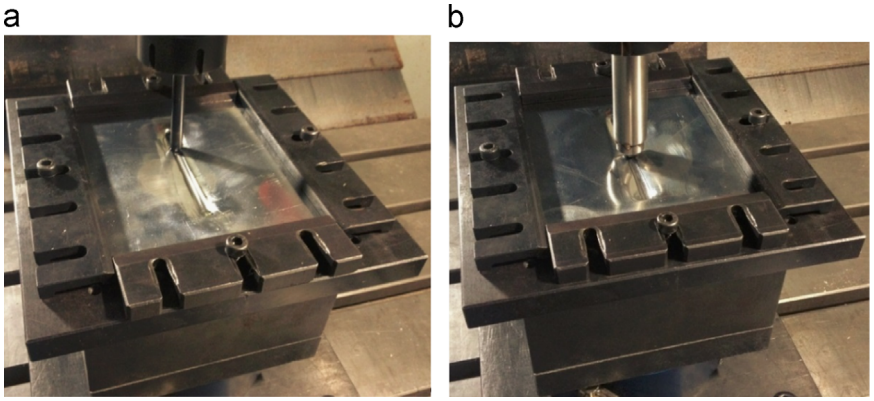

Fig. 9. Friction test by using different tools. (a) Rigid tool and (b) VRB tool.

(2) At the second stage after the 8th pass, when the forming pressure increases to a certain level, the friction indicator of the rigid tool is obviously higher than that of VRB tool.

The friction tests reveal that a lower friction condition can be generated using roller-type tools. This friction reduction is more apparent when the pressure between the tool and sheet metal is high up to a specific level. The frictional effect of the two different tools will be studied in details in the following sections.

3.3. *Surface finish*

Three types of tools (rigid tool, VRB tool and ORB tool) are used to evaluate and compare the surface finish of a truncated cone with wall angle of 45°. Aluminum sheets (AA1100) were employed

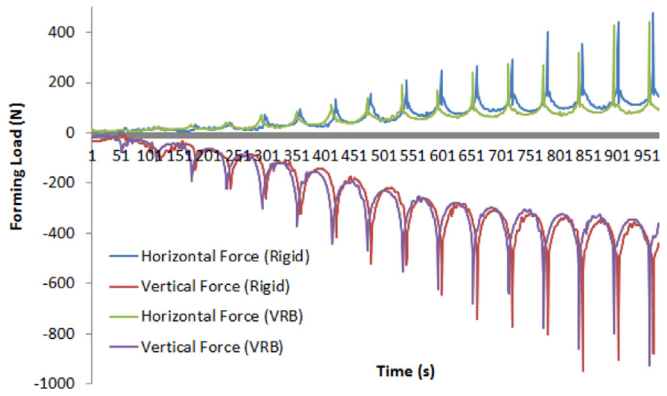

Fig. 10. Comparison of forming load in friction test.

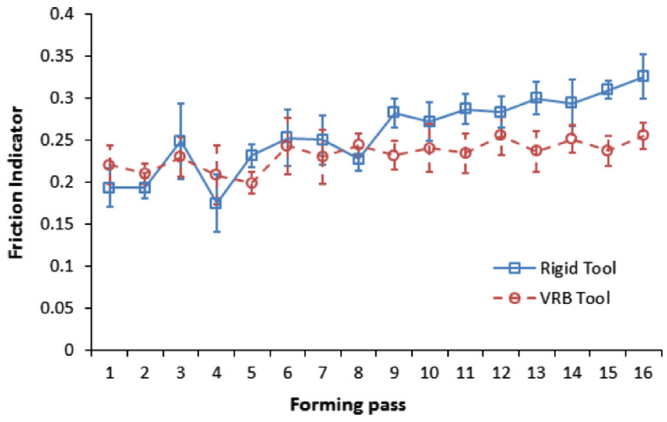

Fig. 11. Friction indicator.

in the study as this material can be easily scratched and it is difficult to obtain good surface quality. Same frictional environment as that in the previous section is employed here. Suggested by Kim et al. [27], a spiral tool path was employed in this study with a step down value of 0.1 mm. For the ORB tool, the tool path was updated according to the algorithm given in Section 2.2. The detailed dimensions of the cone and the finished parts are given in Fig. 12.

Based on the above experimental setup and forming parameters, the parts were fabricated and the roughness were measured and compared as shown in Fig. 13. It was found that no matter what kind of tool is adopted, the roughness of the formed part surface shows increased value compared with that of the original sheet. However, the surfaces processed by ORB tools show lowest roughness R_z and R_a values while those processed by the rigid tool have the maximum values. Comparing the VRB and ORB tools, similar R_z and R_a can be observed without obvious difference. This result proves that the roller ball tools produce better surface finish than the rigid tools.

To further evaluate the tool performance, the surface finish perpendicular to the feed direction was also measured in a length of 2 mm as given in Fig. 14. The surface profile analyses appear to support that the original sheet has a randomly distributed surface profile with a small variation and the shape is basically flat along the whole section. The surface profile processed by rigid tools obviously has more narrow gaps possibly plowed by the tool surface due to relative sliding and no relative rolling between the tool and the sheet. On the contrary, the surfaces processed by both the VRB and ORB tools have less fluctuations and the profile is relatively smooth.

The finished surfaces processed by the rigid tool and the ORB tool were also examined under a microscope. As shown in Fig. 15, tool path traces by the rigid tool are clearly displayed on the surface. Adhesive wear plays a major role in these areas. When sliding friction occurs at the tool–sheet interface, the material is scraped from the sheet and then adhered to the tool surfaces. The scratches would continuously affect the front surfaces and cause successive wear, which leads to some deep gaps as shown in Fig. 15. The surfaces processed by roller-ball tools do not have obvious tool path traces. The experimental results suggest that a better surface finish can be manufactured in rolling friction condition and without lubricant than sliding friction condition and with lubricant. Therefore, the ORB tool is considered to be a better solution for ISF than the conventional rigid tool.

3.4. Formability evaluation

The frictional effect on SPIF formability is evaluated by using both the rigid and the ORB tools. The rigid and ORB tools were chosen for the experiments while the VRB tool was excluded due to two reasons: (1) the VRB tool cannot fully reach forming angle of the designed hyperbolic cone; (2) similar surface finished and profile were observed on the condition of using the ORB and VRB tools, which implies similar frictional effects. Machine oil was used for the rigid tool while no lubricant for the ORB tool. The four aluminum alloy sheet metals mentioned above were used to form a hyperbolic cone given in Fig. 16. Because the forming angle increases gradually with depth, a measure of formability is possible by comparing the depth of fracture [28].

Experimental results in Fig. 17 show that there is obvious difference of fracture depth for different materials: AA1100 could reach 49 mm approximately whilst AA6111 only 16 mm. The fracture depths of AA2024, AA5052 and AA6111 using the ORB tool are much deeper than those made by the rigid tool, indicating that the ORB tool achieves better ISF formability. The fracture depth of AA2024 by ORB tool received the largest difference as of 8.5 mm compared with that by rigid tool. Since only the friction condition was changed except while the forming parameters were kept the same, the friction condition plays a leading role in this difference of the fracture depth.

One exception of the formability test is the material AA1100, from which the difference of the fracture depth by two tools is quite small. The reason for this might account for AA1100's excellent formability, allowing for a final wall angle of 80° in the hyperbolic part. As mentioned before, the wall angle of 80° exceeds the maximum achievable forming angle of the ORB tool. The interference between the tool and sheet caused obvious tool marks on the deformed part as shown in Fig. 17(b). As expected, the tool scratches lead to earlier fracture of part and the fracture depth of ORB tool is slightly less than that of the rigid tool. The experimental results suggest that ORB tool can increase the ISF formability.

The experimental horizontal and vertical forming loads have been recorded by using JR3 load cell as shown in Fig. 18. For the four sheet metals, the horizontal force increase slowly at the initial stage and maintain at about 100 N in the first 250 s, and then climb up much more quickly. However, as the yield stress for these 4 materials vary, the increasing rates of horizontal forces are different with AA6111 having the largest increasing rate and AA1000 having the smallest one. On the other hand, the vertical force increase more smoothly and reach the maximum values at about 550 s, and then decrease until the fractures appear. This drop may be contributed by larger and larger wall thickness reduction. The vertical forces by the rigid and ORB tool do not shown big difference. However, the horizontal forces by rigid tool for all types of materials clearly show large increase than those by the ORB tool, especially in the first 250 s. After that, as the forming wall becomes steeper, the horizontal force differences between

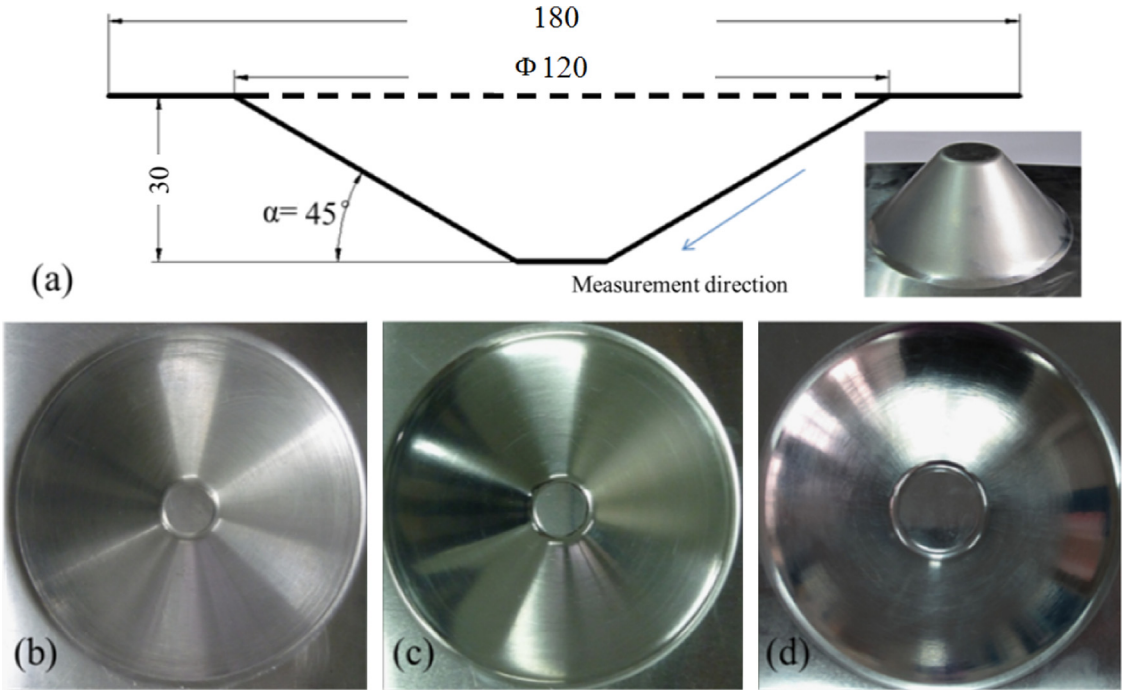

Fig. 12. Cone part geometry (unit: mm): (a) geometric shape of the cone; (b) part processed by rigid tool; (b) part processed by VRB tool; (b) part processed by ORB tool.

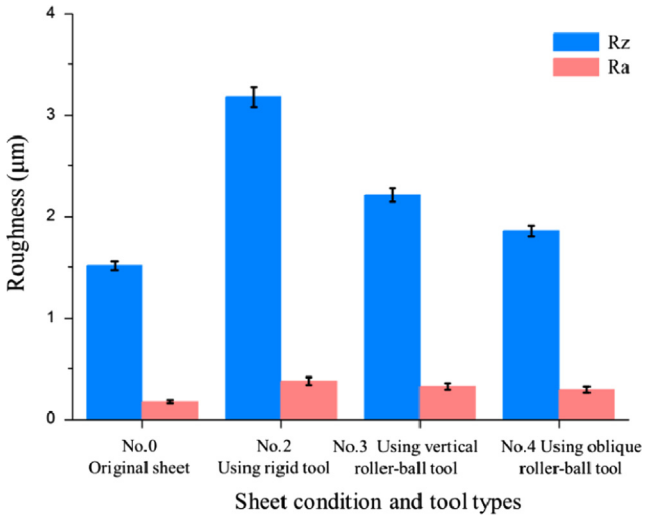

Fig. 13. Roughness bar chart of different tool types and original sheet (30° cone part).

that of rigid tool and that of ORD one are reduced. Furthermore, obvious horizontal force fluctuations of AA1100 and AA6111 by rigid tool are observed, which might be caused by the adhesion of aluminum on the tool and a poor friction condition between the tool and the sheet. However, in the AA2024 and AA5052 materials, the adhesion of material on the tool and the force fluctuation is not obvious.

3.5. *Deformation behavior*

Different formability and forming loads can be observed under different friction conditions. To further investigate the cause of the improved formability, the material deformation behavior under different friction conditions was also studied. In experiments, small holes with a diameter of 0.4 mm were drilled in the sheet by using the micro-EDM process. Fig. 19 shows the cross section of drilled holes on a blank with thickness of 1 mm. In order to reduce the local deformation caused by these small holes themselves, glue was filled into the holes before SPIF process. In this way, the effect from holes maybe minimized.

Similar to the previous section, different grades of aluminum alloy, including AA1100, AA2024, AA5052 and AA6111 were employed in the analysis. Thus, the frictional effects on through-the-thickness-shear can be evaluated. Fig. 20 shows a typical part processed by using AA1100 with the rigid tool. Note that only the hole marked by red arrow in the figure is analyzed in this work for the reason of consistence: not all of the aluminum materials have a high enough formability allowing them to reach the forming depth that surpasses all of the holes.

After forming, the parts were trimmed around the center of the hole in both meridional and circumferential direction. Then, the trimmed faces were ground along the center line of the hole. In this way, the cross section of the hole can be obtained. Fig. 21 shows the cross section of the hole for AA1100 parts under microscope. Note that the contact surface is the top edge of the pictures illustrated in Fig. 21. In the circumferential direction, obvious shear can be observed for the part made by using the rigid tool. For the part made by the roller-ball tool, there is much less shear appears in the circumferential direction. These results suggest that friction between the tool and the sheet is a major factor that causes the through-the-thickness-shear deformation in the ISF process. Considering the meridional direction as shown in Fig. 21(c) and (d), there is no obvious difference for the cross sections made by both the rigid and the ORB tools. In addition, the cross section of the hole was in a trapezoidal shape without obvious shearing. The formation of this trapezoidal shape is unclear. It may be caused by the bending and unbending of sheet around tool in the forming process.

It can be found from Fig. 21 that the friction generated by different tools caused different degrees of through-the-thickness-shear in the circumferential direction, but there is little difference of deformation in the meridional direction. Since there is little difference in the meridional direction for AA2024, AA5052 and AA6111 materials in Fig. 22, the results for the meridional direction are not presented here. As can be seen in the figure, obvious

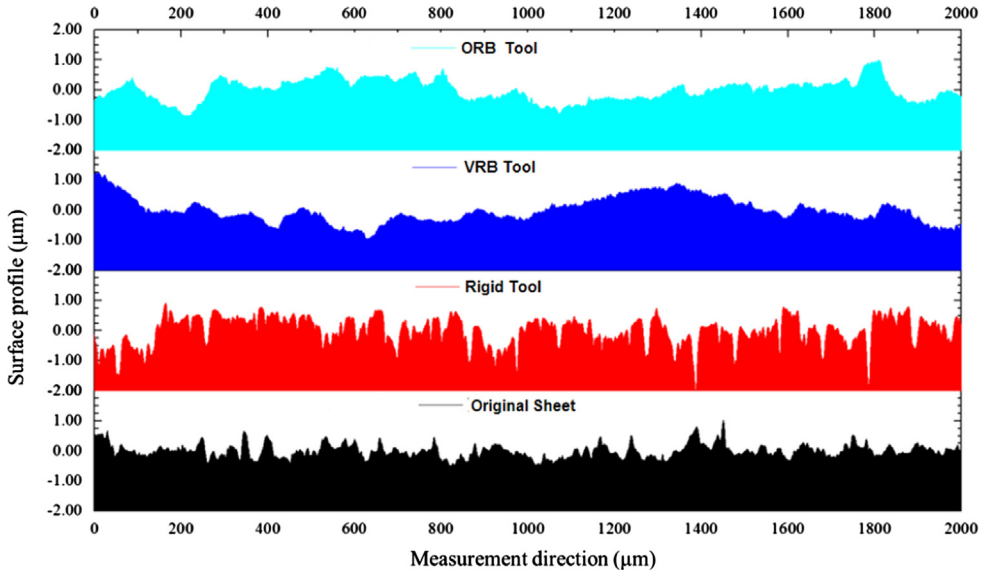

Fig. 14. The part surface profile processed by different tools.

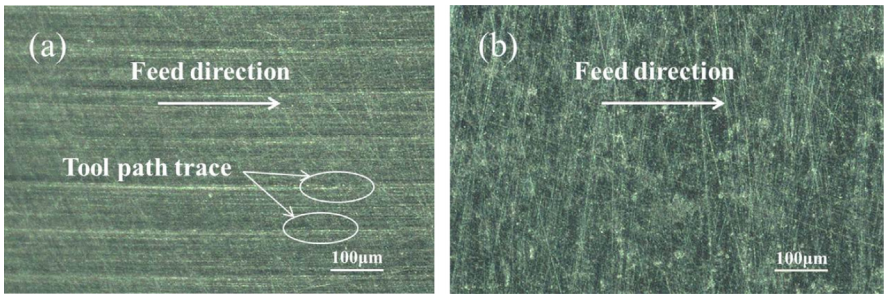

Fig. 15. The surface topographies processed by different tools. (a) Rigid tool (25 ×) and (b) ORB tool.

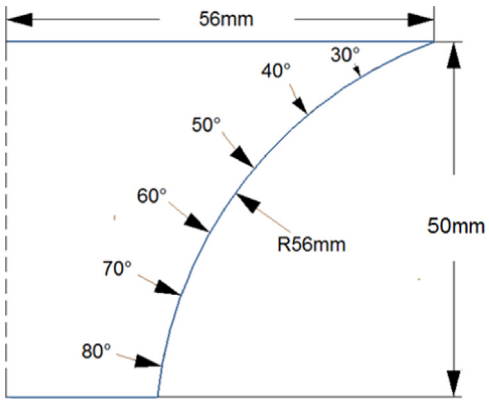

Fig. 16. Geometric shape of hyperbolic cone.

through-the-thickness-shear can be observed for all the parts processed by the rigid tool. Concerning the ORB tool, slight shear can be observed for the AA5052 material, while for AA2024 and AA6111, the shapes of cross-section of the hole are slightly in trapezoidal shape. This result is consistent with the observation obtained from the AA1100 part in that the rigid tool produces higher friction and causes larger through-the-thickness-shear than the ORB tool does during the ISF process. Furthermore, in comparison of the through-the-thickness-shear for different materials, it can be found that the degree of shear may depend on the material type: the shear of AA6111 parts is smaller than the other three materials.

To summarize the above experiments, it can be concluded that the dominate deformation is the stretching in the meridional direction whilst there may be considerable shearing in the circumferential direction. However, the shearing in the meridional direction is not obvious. Similar results are obtained by Jackson and Allwood [24]. In their research, significant stretching in the radial–axial plane and the shear in the tool direction were observed for forming a truncated cone using a copper plate with a thickness of 3.1 mm. This work not only further confirms the basic deformation mechanism of SPIF, but also signifies the friction effect as the major cause of through-the-thickness-shear in the tool motion direction.

4. Discussion the role of friction and through-the-thickness-effect

In this section, different friction conditions and how they affect the forming load as well as the formability are analyzed and discussed from the stress state point of view.

4.1. Computation of stress state in the ISF forming process

In the ISF process, the tool moves along a pre-defined tool path and stretches the sheet locally around the contact area between the tool and sheet. In order to analyze the material deformation in

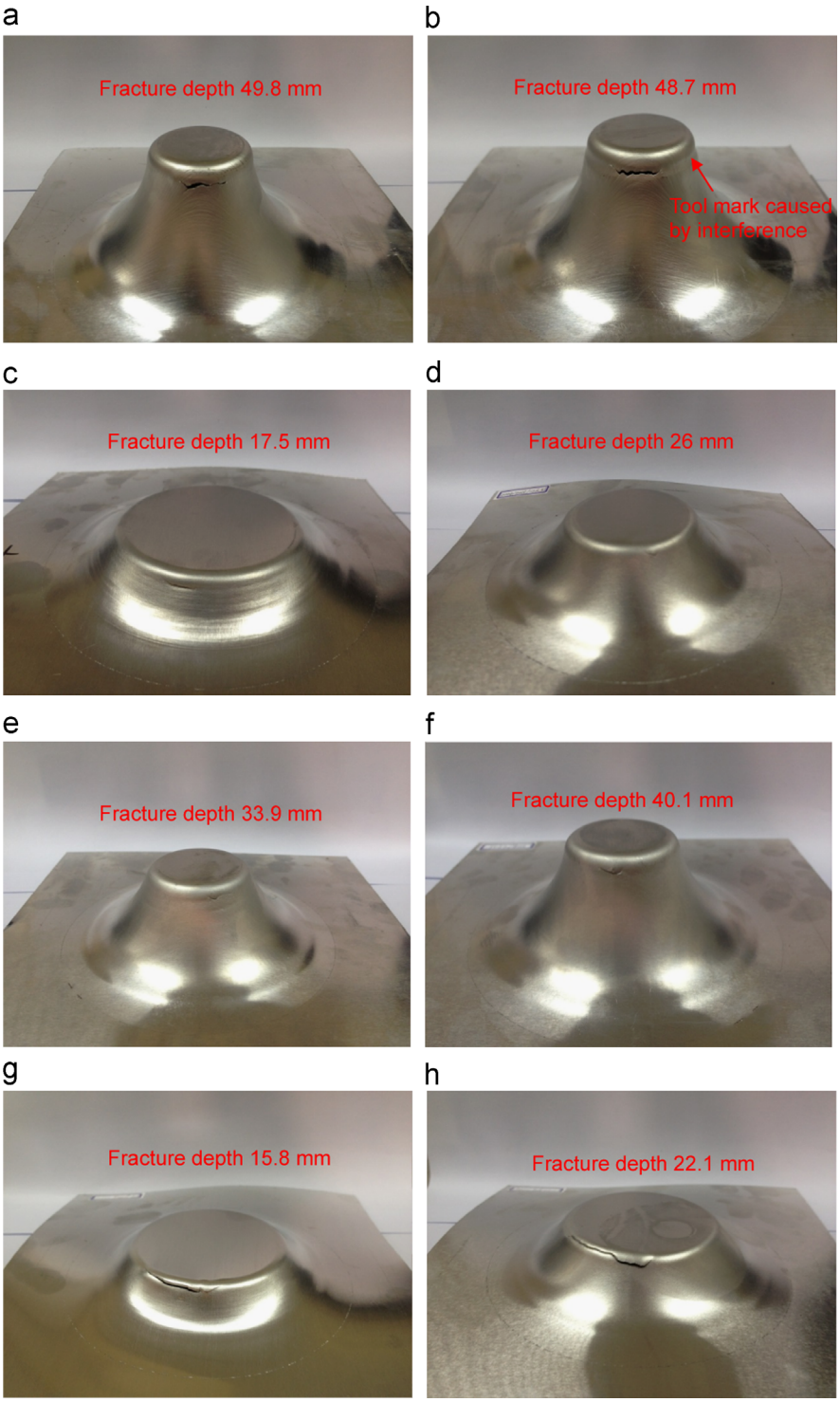

Fig. 17. Comparison of fracture behavior for different aluminums under both rigid and ORB tools. (a) AA1100 with rigid tool, (b) AA1100 with ORB tool, (c) AA2024 with rigid tool, (d) AA2024 with ORB tool, (e) AA5052 with rigid tool, (f) AA5052 with ORB tool, (g) AA6111 with rigid tool, and (h) AA6111 with ORB tool.

the ISF process, stress analysis based on a membrane approach proposed by Silva et al. [29,30] is implemented in this study. In the contact area, part of the sheet is touching the tool's ball-nose surface, as shown in Fig. 23(a). Other than the contact area, the inclined wall of the part may also experience plastic or elastic deformation depending on the forming condition. In this way, the area neighboring to the contact zone on the inclined wall is also analyzed. The contact area is defined as region A while the inclined wall that neighboring to the contact area is defined as region B. Similar definition of the sheet area in the ISF analysis may be referring to [30,31], which is depending on the contact status and the corresponding stress state. In order to analyze the stress state in the ISF process, a small element through the sheet in the contact zone is chosen for the analysis. Fig. 23(b) illustrates the detailed view of the small element (in red color) in the contact zone. As shown in Fig. 23(c), three stress components σ_r, σ_θ and σ_ϕ are defined along the directions of r, θ and ϕ, respectively. Concerning the shear stress, as observed in the experiment, the shear stress $\tau_{r\theta}$

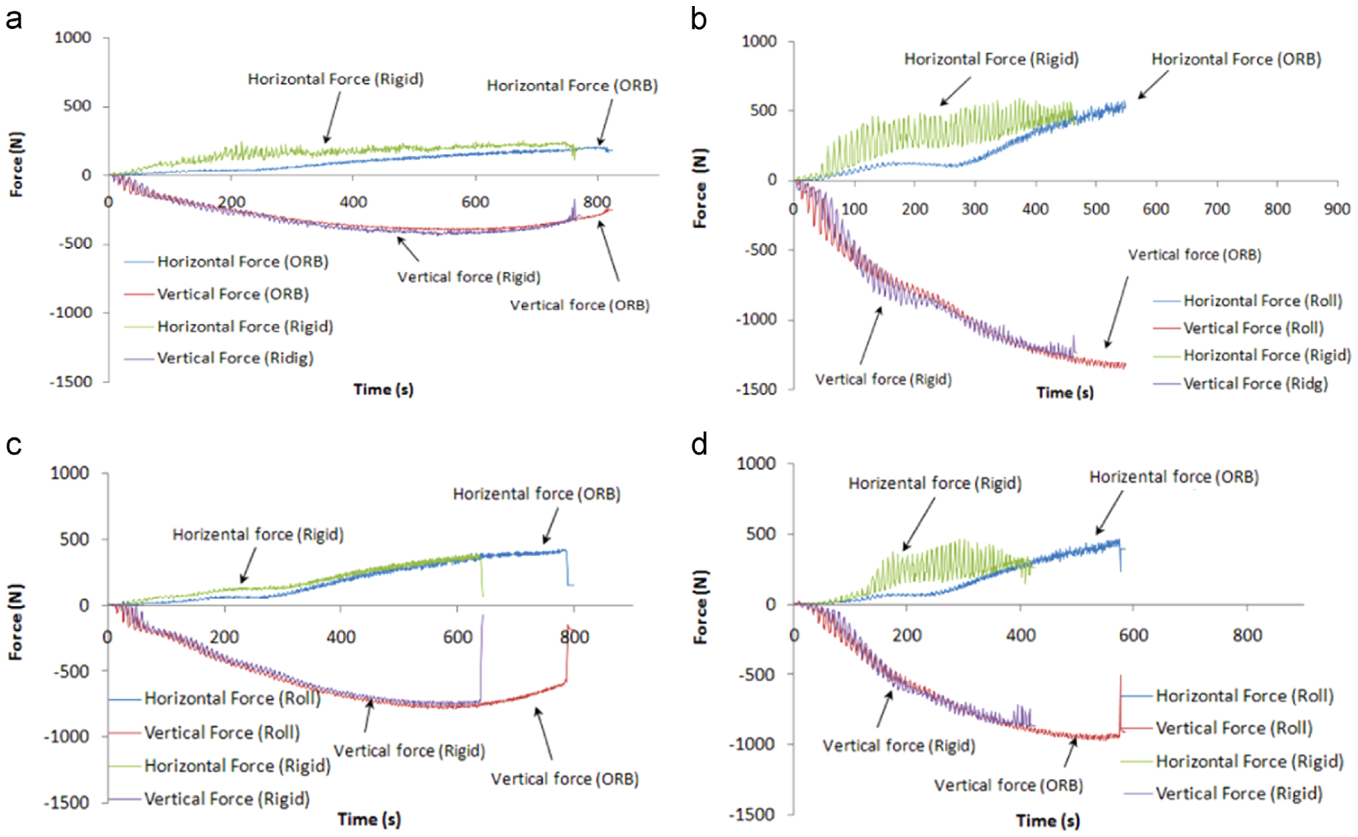

Fig. 18. Comparison of forming loads for both rigid and ORB tools. (a) AA1100, (b) AA2024, (c) AA5052, and (d) AA6111.

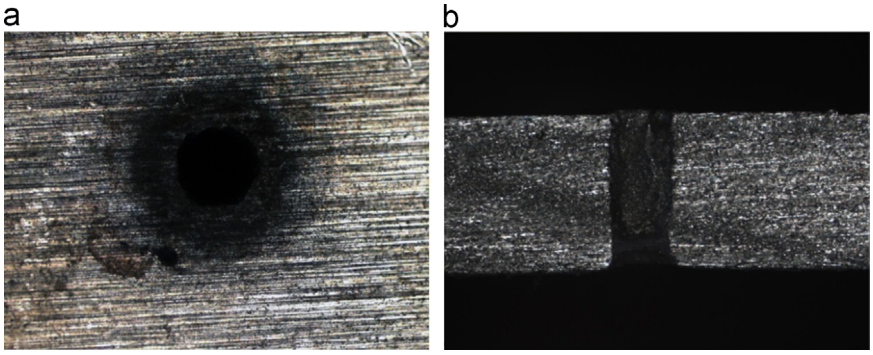

Fig. 19. The initial small hole on the blank. (a) Top view and (b) section view.

Fig. 20. Hyperbolic cone with small holes. (For interpretation of the references to color in this figure, the reader is referred to the web version of this article.)

causes the obvious through-thickness shear in the circumferential direction, which can be considered as the dominant shear effect in the SPIF process whilst the other two shear stress components $\tau_{r\phi}$ and $\tau_{\theta\phi}$ can be ignored since they do not appear to cause obvious material plastic deformation.

In this way, the assumptions of the theoretical analysis can be summarized as follows:

(1) Membrane approach is employed: no bending effect is considered in the analysis as the sheet is very thin comparing to the tool radius.
(2) Only the shear stress in the circumferential direction $\tau_{r\theta}$ is considered: the other two shear component $\tau_{r\phi}$ and $\tau_{\theta\phi}$ are neglected.
(3) σ_r is not related to θ: the through thickness normal stress applied by tool pressure are evenly distributed along the circumferential direction on the contact surface.

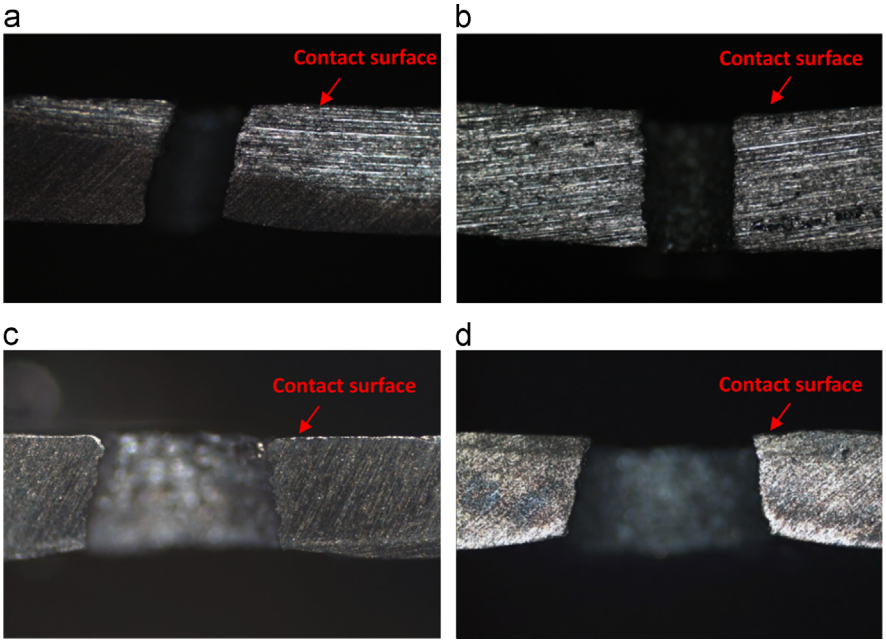

Fig. 21. The deformation of small holes for AA1100 after ISF forming process. (a) Rigid tool at circumferential section, (b) roll ball tool at circumferential section, (c) rigid tool at meridional section, and (d) roll ball tool at meridional section.

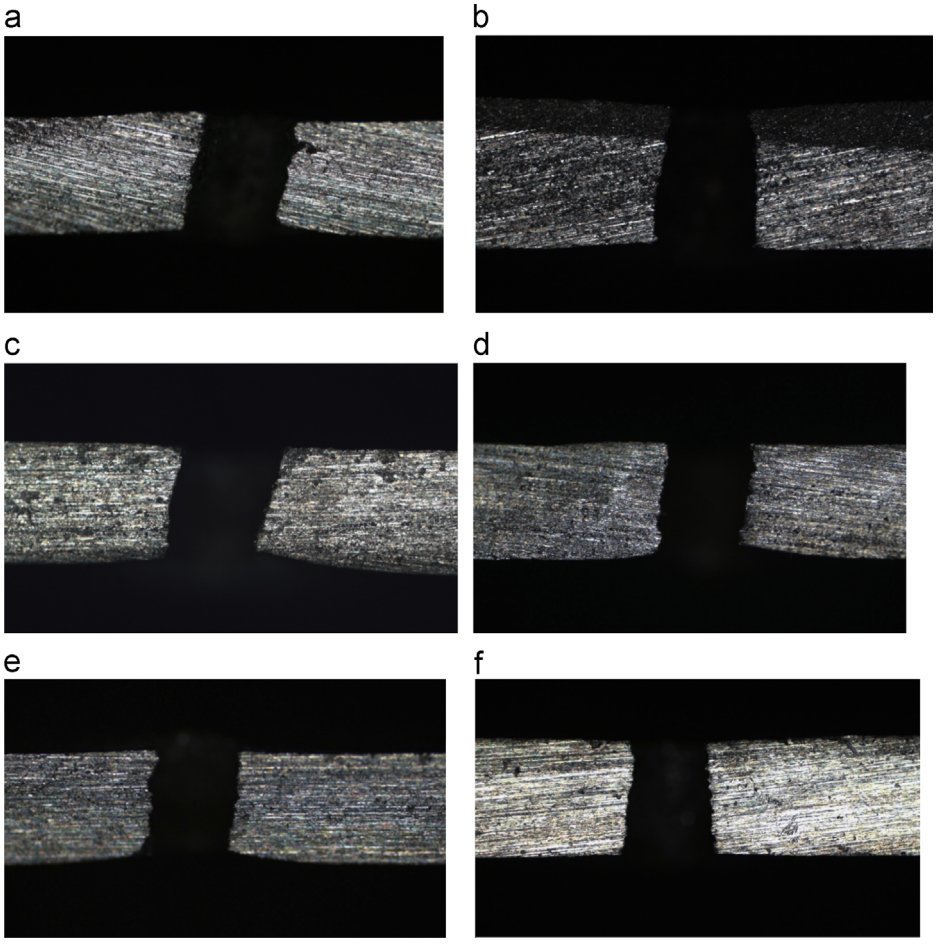

Fig. 22. The deformation of small holes along circumferential direction. (a) AA2024 with rigid tool, (b) AA2024 with ORB tool, (c) AA5052 with rigid tool, (d) AA5052 with ORB tool, (e) AA6111 with rigid tool, and (f) AA6111 with ORB tool.

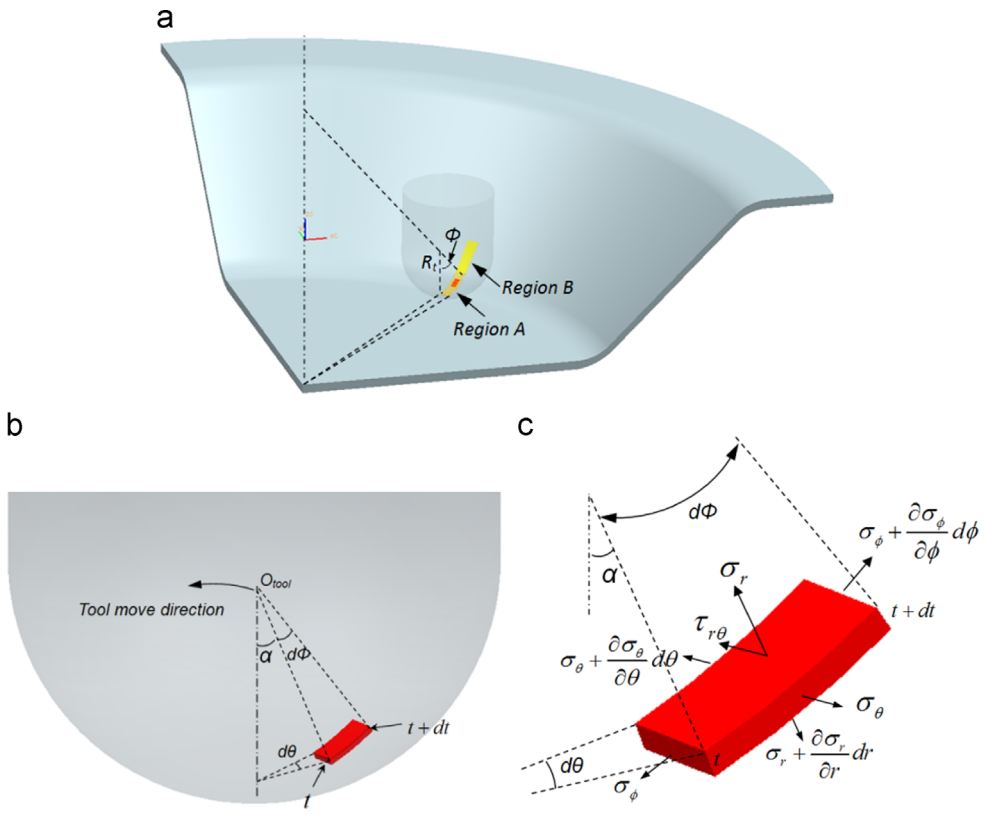

Fig. 23. Schematic representation of ISF forming. (a) Overview, (b) small element in Region A, and (c) stress components. (For interpretation of the references to color in this figure, the reader is referred to the web version of this article.)

In coherence of the membrane approach, the friction condition can be addressed as

$$\tau_{r\theta} = \mu \sigma_r \tag{5}$$

where μ is the friction coefficient between tool and sheet.

Along the circumferential direction, the force equilibrium equation can be expressed as

$$\sigma_\theta r_t d\phi \left(t + \frac{dt}{2}\right) - \mu \sigma_r r_t d\phi r_t d\theta = (\sigma_\theta + d\sigma_\theta) r_t d\phi \left(t + \frac{dt}{2}\right) \tag{6}$$

By ignoring the higher order terms, this equation can be simplified as

$$d\sigma_\theta = -\mu \sigma_r \frac{r_t d\theta}{t} \tag{7}$$

As σ_r is not related to θ, and assuming that the circumferential stress is approximately zero i.e. $\sigma_\theta \approx 0$ at the boarder of contact zone (θ=0). Using these boundary conditions, the circumferential stress σ_θ can be given by

$$\sigma_\theta = -\mu \sigma_r \frac{r_t \theta}{t} \tag{8}$$

Similarly, along the thickness direction, the equilibrium equation can be given by

$$\sigma_r r_t d\theta r_t d\phi + \sigma_\theta r_t d\phi \left(t + \frac{dt}{2}\right) \sin \frac{d\theta}{2} + (\sigma_\theta + d\sigma_\theta) r_t d\phi \left(t + \frac{dt}{2}\right) \sin \frac{d\theta}{2}$$
$$+ \sigma_\phi r_t d\theta t \sin \frac{d\phi}{2} + (\sigma_\phi + d\sigma_\phi) r_t d\theta \left(t + \frac{dt}{2}\right) \sin \frac{d\phi}{2} = 0 \tag{9}$$

which can be simplified as

$$\sigma_r = -\sigma_\theta \frac{t}{r_t} - \sigma_\phi \frac{t}{r_t} \tag{10}$$

In the above analysis, Eqs. (7) and (10) are similar to those obtained by Silva et al. [29], as the equilibrant conditions are the same. Based on these basic equilibrant equations, substituting Eq. (8) into Eq. (10), the following equation is obtained as

$$\sigma_\phi = \frac{r_t}{t}(\mu\theta - 1)\sigma_r \tag{11}$$

Based on Eqs. (5), (8) and (11), the Von Mises stress of the sheet metal can be calculated by

$$\begin{aligned} \overline{\sigma} &= \frac{1}{\sqrt{2}} \sqrt{(\sigma_r - \sigma_\theta)^2 + (\sigma_r - \sigma_\phi)^2 + (\sigma_\theta - \sigma_\phi)^2 + 6\tau_{r\theta}^2} \\ &= -\sqrt{1 + \frac{r_t}{t} + \left(\frac{r_t}{t}\right)^2 - 3\mu\theta \left(\frac{r_t}{t}\right)^2 + 3\mu^2\theta^2 \left(\frac{r_t}{t}\right)^2 + 3\mu^2}\, \sigma_r \\ &= -k_1 \sigma_r \end{aligned} \tag{12}$$

where

$$k_1 = \sqrt{1 + \frac{r_t}{t} + \frac{r_t^2}{t^2} - 3\mu\theta \left(\frac{r_t}{t}\right)^2 + 3\mu^2\theta^2 \left(\frac{r_t}{t}\right)^2 + 3\mu^2} \tag{13}$$

k_1 can be considered as a ratio between the $\overline{\sigma}$ and the normal stress component σ_r, which is related to friction and geometrical parameters.

By observing Eq. (13), it can be found that factor k_1 could be affected by a few forming parameters including the actual sheet thickness t, the tool radius r_t, the circumferential angle θ and the friction coefficient μ. Holding the tool radius r_t constant, Fig. 24 plots the function k_1 with respect to the other three parameters, namely μ, θ and t. As can be seen from the figure, $k_1$decreases with the increase of the friction coefficient μ. This relationship suggests that if the yield stress is constant, the increase of friction coefficient causes larger through thickness normal stress σ_r. In addition, it may also be suggested that if the circumferential contact angle increases, i.e., at the corner of ISF part such as a pyramid design, the through thickness normal stress σ_r also becomes higher.

Concerning the non-contact area (Region B), since there is no direct contact between the tool and Region B, the stress component in the thickness direction σ_r can be considered as $\sigma_r=0$. Due to the equilibrium between Regions A and B, the stress component in the meridional direction σ_ϕ^B will be the same as Region A. Concerning the deformation state, many research suggested that the Region B is under plane strain conditions with $\varepsilon_\theta^B=0$: Silva et al. [30] suggested that the material deformation around the contact area on the side wall in forming a pyramid shape was under plane strain condition through FE approach. The authors also observed the plane strain deformation of sheet in Region B through the measurement of strain using video strain gauge during forming of a truncated cone [31]. Based on the above evidence, the stress σ_θ^B can be given by

$$\sigma_\theta^B=\frac{1}{2}(\sigma_t^B+\sigma_\phi^B)=\frac{1}{2}\sigma_\phi^B \tag{14}$$

If the sheet metal yields in this area, the yield stress must satisfy the condition as

$$\begin{aligned}\overline{\sigma}_B&=\frac{1}{\sqrt{2}}\cdot\sqrt{(\sigma_t^B-\sigma_\phi^B)^2+(\sigma_t^B-\sigma_\theta^B)^2+(\sigma_\phi^B-\sigma_\theta^B)^2}\\&=\frac{\sqrt{3}}{2}\sigma_\phi^B\\&=\frac{\sqrt{3}}{2}\frac{r_t}{t}(\mu\theta-1)\sigma_r\\&=-k_2\sigma_r\end{aligned} \tag{15}$$

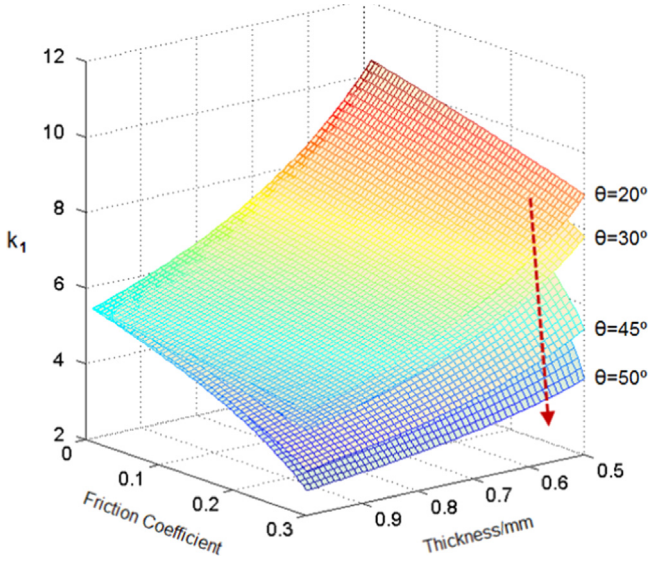

Fig. 24. Relationship between k_1 and other factors.

where

$$k_2=\frac{\sqrt{3}}{2}\frac{r_t}{t}(1-\mu\theta) \tag{16}$$

Assuming that the tool radius $r_t=5$ and thickness $t=1$ at the connecting area between Regions A and B, Fig. 25 plots the relationship between k_1 and k_2 respecting to the friction coefficient under the same μ and θ. It is obvious that $k_1>k_2$, suggesting that the contact area will reach yielding point earlier than the non-contact area under same forming force. In another word, the non-contact area will not reach the yield point when the forming force maintains at the level that causes the contact area to yield. In this way, the plastic deformation only occurs around the contact area with the tool. As shown in Fig. 25(a), when the circumferential contact angle is small, i.e. $\theta=20^\circ$, the gap between k_1 and k_2 increases when the friction coefficient gets larger. When the circumferential contact angle is larger as given in Fig. 25(b) and, this trend is not obvious if the friction coefficient is too small, i.e. $\mu<0.1$. However, if $\mu>0.1$, the discrepancy between k_1 and k_2 is increasing. Considering the friction indicator is around 0.15–0.3 as given in Fig. 11, it can be concluded that the increase of friction will further increase the gap between k_1 and k_2, which potentially enhance the deformation stability in SPIF process.

Concerning the forming force, assume that the contact area between the tool and the small element is S_c, where S_c is only related to geometrical parameters. As this contact area is small, the contact force can be calculated by

Vertical force:

$$f_Z=\sigma_r S_c\cos\frac{\phi}{2}=\frac{\overline{\sigma}}{k_1}S_c\cos\frac{\phi}{2} \tag{17}$$

Horizontal force:

$$f_H=\sqrt{f_r^2+f_\theta^2}=\sqrt{\left(\sigma_r S_c\sin\frac{\phi}{2}\right)^2+(\mu\sigma_r S_c)^2}=\frac{\overline{\sigma}}{k_1}S_c\sqrt{\sin^2\frac{\phi}{2}+\mu^2} \tag{18}$$

In the above equations, the yield stress $\overline{\sigma}$ and contact area S_c are irrelevant to the friction coefficient μ. These terms may be moved to the left side of the equation. As a result, "normalized" force components can be calculated:

$$\frac{f_Z}{\overline{\sigma}S_c}=\frac{1}{k_1}\cos\frac{\phi}{2} \tag{19}$$

$$\frac{f_H}{\overline{\sigma}S_c}=\frac{1}{k_1}\sqrt{\sin^2\frac{\phi}{2}+\mu^2} \tag{20}$$

The defined normalized forces can be considered as the ratio between contact pressure and yield stress. Under a typical ISF condition with tool radius $r_t=5$ mm and forming angle $\phi=60^\circ$, the relationship between the normalized forming forces and the friction coefficient can be expressed as given in Fig. 26. As shown

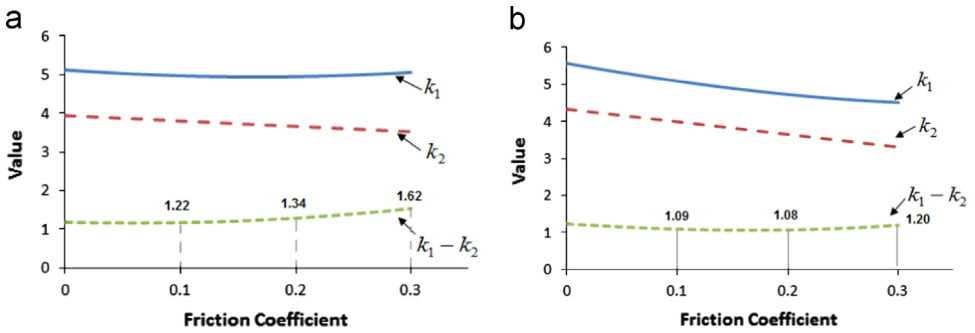

Fig. 25. Relationship between k_1 and k_2 under different friction conditions. (a) $\theta=20^\circ$ and (b) $\theta=45^\circ$.

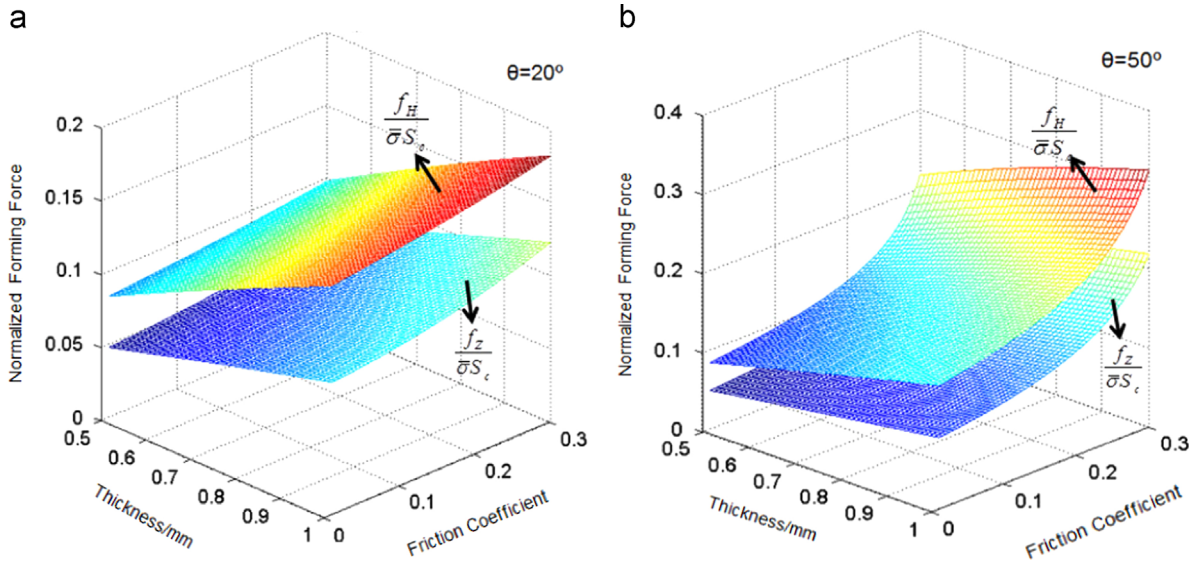

Fig. 26. Relationship between normalized forces and other factors. (a) $\theta=20^{\circ}$ and (b) $\theta=50^{\circ}$.

in the figure, both horizontal and vertical forces are nonlinear in the 3D space. The shape of surface depends on the circumferential contact angle between the tool and the sheet. These forces increase with the increase of friction coefficient. However, the horizontal force is more sensitive than the vertical force: an increase in the friction coefficient leads to a greater increase of the horizontal force component and smaller increase of vertical force component, especially when the circumferential contact angle is small. The result obtained from the stress analysis suggests the same trend of force variation under different friction conditions as presented by the experiments shown in Fig. 18: with the increase of friction coefficient, the horizontal force increases while the vertical force is less sensitive. The validation of force variation trend suggests the effectiveness of the developed model.

Concerning the formability, many researchers employed the strain based approaches such as forming limit diagram (FLD) to analyze the ISF formability [32]. However, in this work, the material deformation difference is shear strain caused by the friction, the use of the strain based approach is difficult as conventional FLD does not consider the through-the-thickness-shear strain. Considerable evidences suggest that the formability is related to triaxial stresses. The role of stress triaxiality in the growth rate of micro voids was early identified by McClintock [33]. Silva et al. [30] employed the stress triaxiality to predict the fracture of sheet in the ISF process. In this work, the ISF formability is evaluated also from the stress triaxiality point of view.

The hydrostatic stress, as mean stress can be firstly calculated as

$$\sigma_m=\frac{1}{3}(\sigma_r+\sigma_\theta+\sigma_\phi)=\frac{1}{3}\left(1-\frac{r_t}{t}\right)\sigma_r=\frac{1}{3}\left(\frac{r_t}{t}-1\right)\frac{\overline{\sigma}}{k} \tag{21}$$

Based on Eqs. (12) and (21), the stress triaxiality can then be calculated by

$$\eta=\frac{\sigma_m}{\overline{\sigma}}=\frac{1}{3}\frac{r_t-t}{tk} \tag{22}$$

Eq. (22) contains complex relationship between stress triaxiality and other parameters. Similar to the previous case, given that the tool head radius r_t is 5 mm and the wall angle is 60°, the stress triaxiality η can be plotted as shown in Fig. 27. It can be found that no matter how much the thickness and circumferential angle are, the stress triaxiality increases with the increase of friction coefficient, indicating lower formability in the SPIF process. The

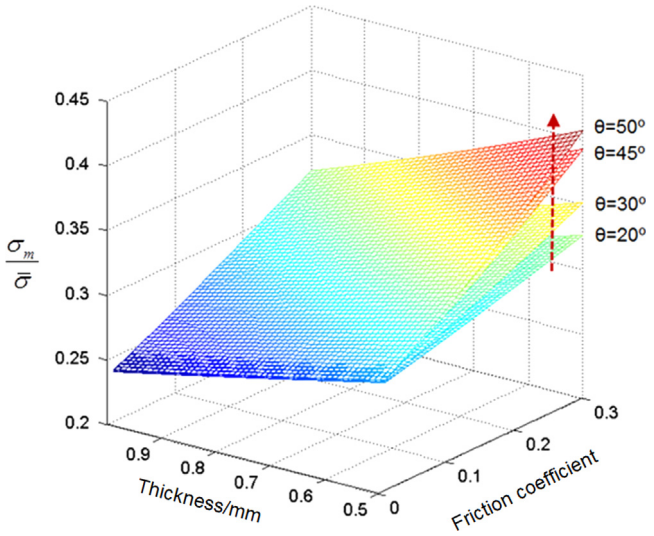

Fig. 27. Relationship between stress triaxiality and other factors.

calculated relationship between stress triaxiality and friction coefficient is similar to that observed from experiments in Section 3.5, the ORB tool leads to higher formability than the rigid tool for most of the aluminum sheets. Furthermore, the proposed stress triaxiality model also implies another fracture related derivation: the circumferential contact angle θ will also influence the formability. Larger θ (normally at the corner of part) will result in higher stress triaxiality, which potentially reduces the formability in the SPIF process. In order to reduce the influence of θ on the formability, possible solutions include reducing the friction or using a smaller tool to reduce the circumferential contact angle between the tool and sheet.

The developed stress analysis model for the SPIF process provides the similar trends of force and stress triaxiality variation under different friction conditions as those observed in the experiments. The consistent results have proved the robustness of the developed analytical model. Although some simplifications are made, this model gives a reasonable explanation for the experimental results, especially in describing the relationship among the forming force, formability and friction coefficient. Concerning the SPIF formability, the developed model may explain the two contrary effects from friction: from one hand, increasing

the friction would increasing the stability and suppress the necking; on the other hand, increasing the friction would also increase the stress triaxiality and reduce the formability. The final role of the friction depends on the contributions of the two effects. In the implemented experiments, the effect of stress triaxiality is more significant than the effect of stability, thus the friction negatively impact the SPIF formability.

4.2. Discussion on the through-the-thickness-shear effect

The variation in trend of the forming load obtained from both analytical analyses suggests that smaller friction leads to lower forming force, especially in the horizontal direction. In addition, the developed model also suggests that smaller friction results in lower stress triaxiality, which potentially increases the SPIF formability. The analytical derivations are consistent with the experimental results especially for AA2024, AA5052 and AA6111 material. Concerning the effect of through-the-thickness-shear in the ISF process, experimental results presented in Figs. 21 and 22 suggest that by using the rigid tool which will generate higher friction, a larger through-the-thickness-shear can be observed in the tool moving direction. At the same time, the fracture depth of parts processed by using the rigid tool is lower than that of the ORB tool. These results may imply that the through-the-thickness-shear has a negative effect on the formability of SPIF process. This argument may also be supported by Cao's work regarding the through-the-thickness-shear and use of a shear-modified GTN model [34]. In their research, the formability in SPIF processes may be reduced by introducing the through-the-thickness-shear. However, a different opinion on the effect of through-the-thickness-shear is from Allwood's work [20,24,35]. Their research suggested that the through-the-thickness-shear effect increases the sheet formability based on the calculation of an extended forming limit diagram (FLD) through Marciniak–Kuczynski (M–K) analysis. Another opinion comes from the studies done by Skjoedt et al. [36,37] on the effect of forced tool rotation or free rotation showed no influence on the overall formability. Their observation leads to the conclusion that the influence of friction resulting from the contact between the tool and the sheet is negligible. Silva et al. [30] also suggested that the through-the-thickness-shear effect is not very significant in the SPIF process. The above literatures gave different opinions on the role of through-the-thickness-shear in the SPIF process. Thus the effect of the through-the-thickness-shear on SPIF process is still questionable. Concerning the theoretical analysis in Section 4.1, it was suggested that the increasing of through-the-thickness-shear results in two contrary effects, from one hand, the sole yielding of the sheet metal in contact zone increases deformation stability and suppresses necking; on the other hand, the increasing of stress triaxiality decrease the formability. In addition, another un-neglecting frictional effect is the surface roughness. Surface topography study given in Fig. 15 shows obvious tool marks or even scratches on the sheet surface processed by the rigid tool. These scratches may also reduce the formability in the SPIF process. The high friction between the tool and sheet not only causes larger shear but also produces poorer surface finish. Although it is difficult to quantitatively evaluate the impact of surface finish on the overall formability, the experimental work in this paper suggested that the increased friction negatively affect the SPIF formability while the positive effect of stability is negligible.

Furthermore, not only does the through-the-thickness-shear, but also other effects in the SPIF process, such as bending-under-tension (BUT), have also been proven to have positive effects on the SPIF stability by suppressing the necking in the forming process [38]. In addition, serrated strain paths arising from cyclic loading and local plastic deformation may be the other important reasons for increasing the SPIF stability [39]. The SPIF process contains complex forming mechanisms in which the effects from stretching, bending, shearing, cyclic loading and localized deformation has their respective contributions to the deformation process. The significance of each effect depends on its own weighting in the SPIF process. Although the detailed weighting of each factor may vary, the through-the-thickness-shear might not be the dominate one. Considering the fact that SPIF formability is evaluated by sheet fracture other than necking, recent research on the formability limits by fracture in sheet metal forming suggested that fracture loci is controlled by the reduction in thickness or distortion [40], which further confirms the minor role of through-the-thickness-shear in the overall formability in SPIF process.

Concerning the fact that the formability of the SPIF process is higher than the conventional stamping or deep drawing, this study suggests that as through-the-thickness-shear is considered as a secondary effect, the cause of the increased deformation stability and formability in the SPIF process might be largely due to BUT or other deformation mechanisms, while the through-the-thickness-shear might only have limited contribution. Further study is necessary to have in-depth investigation on the cause of increased formability in the SPIF process.

5. Conclusions

In this work, the friction effect in the SPIF process has been investigated based on a newly developed ORB tool. The ORB tool shows obvious advantages in reducing the friction between the tool and sheet, and it improves the surface finish even when lubricants are not used. By drilling small holes in the sheet metal, the through-the-thickness-shear was investigated under different friction conditions. Further investigations on SPIF formability have also been implemented. These experiments confirm the significance of tool friction during the SPIF process in terms of: (1) forming force, (2) surface finish and (3) SPIF formability. In an effort to explain the experimental results, an analytical model has been established based on the stress state. The analytical derivation provides a better understanding on how the friction affects the stress state and corresponding forming load, as well as the formability in the SPIF process. Finally, the role of through-the-thickness-shear in the ISF process has also been discussed.

The conclusions are summarized as follows:

(1) Friction in SPIF process can be reduced by replacing the conventional rigid tool with roller-based tool. The advantages of the roller-based tool include better surface finish, lower forming load and higher formability.
(2) Friction affects the material deformation behavior in the SPIF process. While the dominant deformation mechanism in SPIF process is sheet stretching along the meridional direction, high friction causes considerable through-the-thickness-shear along the tool moving direction. However, the shear along the meridional direction is not obvious in the experiments.
(3) Friction also affects SPIF deformation stability and formability. Through an analytical model, it was suggested that through-the-thickness-shear caused by friction results in contrary effects: higher shear stress not only potentially increases the SPIF deformation stability, but also increases the stress triaxiality and reduces the formability at the same time.
(4) The significance of through-the-thickness-shear might be reduced due to the two contrary effects. The effect from through-the-thickness-shear might be hidden in the other SPIF deformation mechanisms such as BUT, serrated strain paths or even bad surface finish due to high friction. In this

way, the through-the-thickness-shear may be considered as a secondary effect in the SPIF process.

It is also worthwhile to point out that the results obtained in this work are based on the tests of different types of aluminum sheets. Future research is necessary to investigate the frictional effects and the corresponding through-the-thickness-shear effect during the ISF process of other materials.

Acknowledgment

The research work was supported by the Marie Curie International Incoming Fellowship within the 7th European Community Framework Programme (628055 and 913055) and the Engineering and Physical Science Research Council (EP/L02084X/1).

References

[1] P. Roux, Machines for Shaping Sheet Metal, United States Patent Office, 1960.
[2] E. Leszak, Apparatus and Process for Incremental Dieless Forming, United States Patent Office, 1967.
[3] H. Iseki, K. Kato, S. Sakamoto, Flexible and incremental sheet metal forming using a spherical roller, in: Proceedings of 40th JJCTP 41–44, 1989 (in Japanese).
[4] S. Matsubara, Incremental backward bulge forming of a sheet metal with a hemispherical head tool, J. Jpn. Soc. Technol. Plast. 35 (1994) 1311–1316.
[5] B.T. Araghi, G.L. Manco, M. Bambach, G. Hirt, Investigation into a new hybrid forming process: incremental sheet forming combined with stretch forming, CIRP Ann. – Manuf. Technol. 58 (2009) 225–228.
[6] R. Malhotra, J. Cao, F. Ren, V. Kiridena, C. Xia, N. Reddy, Improvement of geometric accuracy in incremental forming by using a squeezing toolpath strategy with two forming tools, J. Manuf. Sci. Eng. 133 (2010) 603–611.
[7] J.R. Duflou, B. Callebaut, J. Verbert, H. De Baerdemaeker, Laser assisted incremental forming: Formability and accuracy improvement, CIRP Ann.—Manuf. Technol. 56 (2007) 273–276.
[8] J. Duflou, J. Verbert, B. Belkassem, J. Gu, H. Sol, C. Henrard, A. Habraken, Process window enhancement for single point incremental forming through multi-step toolpaths, CIRP Ann. – Manuf. Technol. 57 (2008) 253–256.
[9] R. Malhotra, J. Cao, M. Beltran, D. Xu, J. Magargee, V. Kiridena, Z.C. Xia, Accumulative-DSIF strategy for enhancing process capabilities in incremental forming, CIRP Ann. – Manuf. Technol. 61 (2012) 251–254.
[10] G. Ambrogio, I. Costantino, L.D. Napoli, L. Filice, L. Fratini, M. Muzzupappa, Influence of some relevant process parameters on the dimensional accuracy in incremental forming: a numerical and experimental investigation, J. Mater. Process. Technol. 153–154 (2004) 501–507.
[11] M. Bambach, B.T. Araghi, G. Hirt, Strategies to improve the geometric accuracy in asymmetric single point incremental forming, Prod. Eng. 3 (2009) 145–156.
[12] B.T. Araghi, G.L. Manco, M. Bambach, G. Hirt, Investigation into a new hybrid forming process: incremental sheet forming combined with stretch forming, CIRP Ann.—Manuf. Technol. (2009) 225–228.
[13] M. Bambach, G. Hirt, S. Junk, Modelling and experimental evaluation of th incremental CNC sheet metal forming process, in: Proceedings 7th COMPLAS, Barcelona, Spain, April 7–10, 2003.
[14] E. Hagan, J. Jeswiet, Analysis of surface roughness for parts formed by computer numerical controlled incremental forming, Eng. Manuf. 218 (2004) 1307–1312.
[15] G. Hussain, L. Gao, N. Hayat, Z. Cui, Y. Pang, N. Dar, Tool and lubrication for negative incremental forming of a commercially pure titanium sheet, J. Mater. Process. Technol. 203 (2008) 193–201.
[16] K. Hamilton, J. Jeswiet, Single point incremental forming at high feed rates and rotational speeds: surface and structural consequences, CIRP Ann.—Manuf. Technol. 59 (1) (2010) 311–314.
[17] M. Durante, A. Formisano, A. Langella, Comparison between analytical and experimental roughness values of components created by incremental forming, J. Mater. Process. Technol. 210 (2010) 1934–1941.
[18] B. Lu, J. Chen, H. Ou, J. Cao, Feature-based tool path generation approach for incremental sheet forming process, J. Mater. Process. Technol. 213 (2013) 1221–1233.
[19] Y.H. Kim, J.J. Park, Effect of process parameters on formability in incremental forming of sheet metal, J. Mater. Process. Technol. 130–131 (2002) 42–46.
[20] J.M. Allwood, D.R. Shoulder, A.E. Tekkaya, The increased forming limits of incremental sheet forming processes, Key Eng. Mater. 344 (2007) 621–628.
[21] P. Eyckens, A. Van Bael, P. Van Houtte, An extended Marciniak–Kuczynski forming limit model to assess the influence of through-thickness shear on formability, in: Proceedings Numisheet 2008 Conference, Interlaken, Switzerland, September 1–5, 2008.
[22] P. Eyckens, , A. Van Bael, R. Aerens, J. Duflou, P. Van Houtte, Small-scale finite element modelling of the plastic deformation zone in the incremental forming process, in: Proceedings Esaform 2008, Lyon, France, April 23–25, 2008.
[23] K.P. Jackson, J.M. Allwood, M. Landert, Incremental forming of sandwich panels, J. Mater. Process. Technol. 204 (2008) 290–303.
[24] K. Jackson, J. Allwood, The mechanics of incremental sheet forming, J. Mater. Process. Technol. 209 (2009) 1158–1174.
[25] P. Eyckens, J. Duflou, A. Bael, P. Houtte, The significance of friction in the single point incremental forming process, Int. J. Mater. Form. 3 (2010) 947–950.
[26] D. Xu, W. Wu, R. Malhotra, J. Chen, B. Lu, J. Cao, Mechanism investigation for the influence of tool rotation and laser surface texturing (LST) on formability in single point incremental forming, Int. J. Mach. Tools Manuf. 73 (2013) 37–46.
[27] K.-K. Kim, M.-C. Kang, J.-S. Kim, Y.-H. Jung, N.-K. Kim, A study on the precision machinability of ball end milling by cutting speed optimization, J. Mater. Process. Technol. 130–131 (2002) 357–362.
[28] G. Hussain, L. Gao, A novel method to test the thinning limits of sheet metals in negative incremental forming, Int. J. Mach. Tools Manuf. 47 (2007) 419–435.
[29] M. Silva, M. Skjoedt, P. Martins, N. Bay, Revisiting the fundamentals of single point incremental forming by means of membrane analysis, Int. J. Mach. Tools Manuf. 48 (2008) 73–83.
[30] M.B. Silva, M. Skjoedt, N. Bay, P.A.F. Martins, Revisiting single-point incremental forming and formability/failure diagrams by means of finite elements and experimentation, J. Strain Anal. Eng. Des. 44 (2009) 221–234.
[31] Y. Fang, B. Lu, J. Chen, D.K. Xu, H. Ou, Analytical and experimental investigations on deformation mechanism and fracture behavior in single point incremental forming, J. Mater. Process. Technol. 214 (2014) 1503–1515.
[32] J. Jeswiet, D. Young, Forming limit diagrams for single-point incremental forming of aluminium sheet, Proc. Inst. Mech. Eng. Part B: J. Eng. Manuf. 219 (2005) 359–364.
[33] F.A. McClintock, A criterion for ductile fracture by the growth of holes, J. Appl. Mech. 35 (1968) 363–371.
[34] J. Smith, R. Malhotra, W.K. Liu, J. Cao, Application of a shear-modified GTN model to incremental sheet forming, AIP Conf. Proc. 1567 (2013) 824–827.
[35] J.M. Allwood, D.R. Shouler, Generalised forming limit diagrams showing increased forming limits with non-planar stress states, Int. J. Plast. 25 (2009) 1207–1230.
[36] M. Skjoedt, N. Bay, E. Endelt, G. Ingarao, Multi stage strategies for single point incremental forming of a cup, in: Proceedings of the 11th ESAFORM Conference on Material Forming, Lyon, France, 2008.
[37] M. Skjoedt, M.B. Silva, P.A.F. Martins, N. Bay, Strain paths and fracture in multi stage single point incremental forming, in: Proceedings of the 9th International Conference on Technology of Plasticity (ICTP 2008), Gyeongju, Korea, 2008.
[38] W.C. Emmens, A.H. Boogaard, Tensile tests with bending: a mechanism for incremental forming, Int. J. Mater. Form. 1 (2008) 1155–1158.
[39] P. Eyckens, S. He, A. Van Bael, P. Van Houtte, J. Duflou, Forming limit predictions for the serrated strain paths in single point incremental forming, in: Proceedings Numiform 07, Portugal, June 17–21, 2007.
[40] K. Isik, M.B. Silva, A.E. Tekkaya, P.A.F. Martins, Formability limits by fracture in sheet metal forming, J. Mater. Process. Technol. 214 (2014) 1557–1565.